ACS APPLIED MATERIALS & INTERFACES

Research Article

www.acsami.org

Organic/Inorganic Composite Membranes Based on Poly(L-lactic-*co*-glycolic acid) and Mesoporous Silica for Effective Bone Tissue Engineering

Panyu Zhou,[†,§] Xiaosong Cheng,[†,§] Yan Xia,[†,§] Panfeng Wang,[†] Kaidian Zou,[‡] Shuogui Xu,*[,†] and Jianzhong Du*[,‡]

[†]Department of Emergency, Changhai Hospital, the Second Military Medical University, 168 Changhai Road, Shanghai 200433, China

[‡]School of Materials Science and Engineering, Tongji University, 4800 Caoan Road, Shanghai 201804, China

ABSTRACT: Fabrication of membranes with excellent biocompatibility and bioactivity remains an important technical challenge in bone tissue engineering. In this paper, poly(L-lactic-*co*-glycolic acid) (PLGA)−SBA15 (Santa Barbara Amorphous 15) composite membranes were prepared by using an electrospinning technique; PLGA was used as a biocompatible and biodegradable polymer and SBA15 was used as a mesoporous silica. The PLGA−SBA15 composite membrane facilitates the cell attachment and the cell proliferation versus pure PLGA membrane where human bone marrow-derived mesenchymal stem cells (hMSCs) were seeded. Furthermore, the analysis of alkaline phosphatase (ALP) activity indicated that this PLGA−SBA15 composite membrane has better osteogenic induction compared with the pure PLGA membrane. Moreover, the presence of SBA15 increased the loading efficiency of the recombinant human bone morphogenetic protein-2 (rhBMP-2) to the membranes. Furthermore, the composite membrane had optimized sustained release of rhBMP-2. Overall, this PLGA−SBA15 composite is an excellent material for bone tissue engineering.

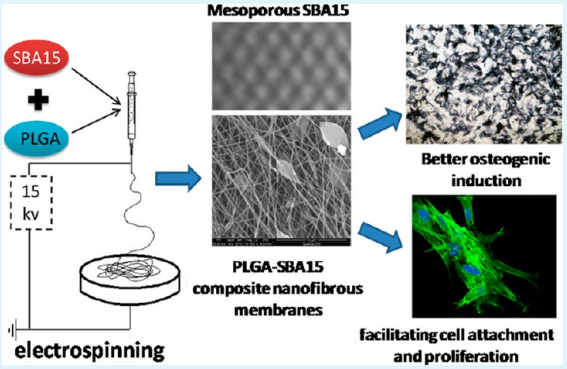

KEYWORDS: *SBA15, PLGA, bone tissue engineering, electrospinning, bioactivity*

INTRODUCTION

Bone scaffold materials can improve cell adhesion, cell proliferation, and cell differentiation into osteoblasts.[1] Such scaffolds usually have an excellent microstructure including well-interconnected pores, which is essential for the transport of nutrients to cells.[2] It also should be nontoxic for clinical applications and easy to fabricate or purchase.[3]

Biocompatible polymers are widely used in tissue engineering such as bone regeneration because polymers have structural memory on the same time scale as tissue growth.[4] For example, FDA-approved poly(L-lactic-*co*-glycolic acid) (PLGA) has been widely used in biomedicine.[5,6] It shows excellent biocompatibility and does not degrade during a short period of time. This is very important for new bone formation.[7] However, for improved bone regeneration and repair, low bioactivity PLGA must be used in combination with other bioactive materials to form a composite scaffold.[8] However, bioactivity and osteoconductivity are suboptimal in the hydrophobic polymer.[9] Thus, it is necessary to add bioactive materials to improve the biological performance of scaffolds. For example, bone morphogenetic protein-2 (BMP-2) is an osteogenic growth factor used widely for bone repair.[10−12] When added into a porous material, it can be released slowly in vivo and can significantly improve bone healing.[13,14]

Ideally, the engineering of a multiphase material should closely mimic the extracellular matrix (ECM) of natural bone and control the release kinetics of growth factors after implantation.[15] Mesoporous materials such as Santa Barbara Amorphous 15 (SBA15, pore sizes of 2−50 nm) can facilitate bone growth via calcium phosphate and promote the differentiation and proliferation of osteoblasts while enhancing the bone−matrix interface strength.[16,17] However, mesoporous materials like other inorganic ceramic materials are highly brittle and inflexible, which hampers bone regeneration.[18]

Thus, composite materials combining a mesoporous particle and a biodegradable polymeric phase were developed to mimic the major ECM of bone; they combine the advantages and minimize the drawbacks of each material in the composite.[19] For example, Shi et al. showed that the addition of mesoporous bioactive glasses (MBG) into poly(L-lactic acid) (PLLA) resulted in enhanced cell attachment with cell spreading and proliferation in a rabbit bone marrow stromal cells (rBMSCs) model.[20] Wu and co-workers fabricated multifunctional porous

Received: August 15, 2014
Accepted: November 14, 2014
Published: November 14, 2014

MBG scaffolds with osteostimulation, drug delivery and antibacterial properties.[21]

Various methods such as self-assembly, electrohydrodynamic printing, bacterial culture and electrospinning have been developed to prepare nanofibrous composite materials for bone regeneration. Of these, electrospinning is very common because of its simplicity and versatility. It produces bone tissue engineering scaffolds that facilitate suitable cell responses (adhesion, proliferation and differentiation).[22−24] Therefore, electrospinning has been used in tissue bioengineering for wound healing.[25,26] Polymer fibers prepared by this technique have a relatively large specific surface area, high porosity and relatively even diameters. This can mimic the structural and functional properties of the ECM. For example, Min et al. fabricated nanofiber nonwoven materials by this technique. This material had high porosity with controllable pore sizes and high surface area-to-volume ratios. These parameters facilitate cell growth, attachment and proliferation.[27]

Here we report a novel PLGA−SBA15 composite membrane to improve cell adhesion, proliferation, and differentiation into osteoblasts. This product was fabricated by electrospinning and offered excellent biocompatibility, bioactivity and osteogenic activity. It is a promising method for fabricating effective bone engineering materials.

EXPERIMENTAL SECTION

Materials. PLGA (M_w = 10 kDa with LA/GA = 50:50) was purchased from Daigang company (Jinan, China). Mesoporous silica SBA15 was prepared according to the literature with a triblock copolymer surfactant.[28] In a typical synthesis, $EO_{20}PO_{70}EO_{20}$ triblock copolymer (Pluronic P123, BASF; 4.00 g) was dissolved in 30 g of distilled water. Then, HCl (120 mL; 2 M) was added with stirring. Next, 8.5 g of tetraethyl orthosilicate (TEOS) at 35−40 °C was added. The resulting gel product reacted for 24 h under gentle stirring. The product was sealed at 100 °C for 48 h. Next, we filtered the solid product and washed it thrice with distilled water. It was air-dried at 100 °C and then calcined again under air at 530 °C for 6 h. This eliminated the surfactant template. The resulting white powder was weighed to calculate yield and termed SBA15.

Characterization. Surface morphology of materials was viewed using scanning electron microscopy (SEM, Quanta 250, FEI, USA) with a field emission gun operating at 20 kV. The same instrument used an X-ray energy dispersive analysis system (EDAX, USA) for chemical analysis.

High resolution transmission electron microscopy (TEM, JEM-2010; JEOL) and small-angle X-ray diffraction (SAXRD) were used to characterize the morphology and microstructure of SBA15. TEM samples were prepared according to our previously reported methods.[29−31]

The Brunauer−Emmett−Teller (BET) method was used to measure the surface area, the nanopore size distribution and the pore volume by N_2 adsorption−desorption isotherms based on Barret−Joyner−Halenda (BJH) analyses (TRISTAR 3000, Micrometrics Instrument Corp., USA).[32,33]

Preparation of Composite Membrane by Electrospinning. The nanofibrous membranes were fabricated by an electrospinning technique.[34] Briefly, we dissolved PLGA in hexafluoroisopropanol (HFP). The final PLGA concentration was 10 wt %. Samples containing SBA15 were doped with nanoparticles in HFP via ultrasonication prior to addition of the polymer. We used dioctyl sulfosuccinate sodium salt at 0.05% w/v as the surfactant. It was dissolved in HFP to facilitate the colloidal stability.

Three types of composite membranes were fabricated with various amounts of SBA15. In all cases, the sample was electrospun at 24.5 kV and room temperature. The distance from the tip to the collector was 15 cm. The product accumulated at the collector plate. The nanofibers were cross-linked in glutaraldehyde vapor at 80 °C for 48 h. The electrospun porous fibrous films were finally dried under vacuum at 80 °C for 12 h.

A commercially available electrospinning device (Advanced Surface Technology, Bleiswijk, The Netherlands) was used for the membrane fabrication. Briefly, 10 mL of the reaction mixture was pumped at 2 mL h^{-1}. A Teflon tubing (0.5 mm ID) was used throughout. The working distance from nozzle to grounded collector was at 12 cm. 18−22 kV of voltage generated a polymer jet. These parameters were tuned with pilot studies to optimize the fabrication for uniform fibrous structures. The resulting fibers were collected, dried and stored over a desiccant. SEM was used to view the morphology via gold sputter coating.

Bioactivity Analysis. The simulated body fluid (SBF) solution was prepared as described previously.[35] Three samples of each film were soaked in 50 mL of SBF solution at 37 °C and a shaking rate of 100 rpm. After 7 days, the specimens were removed and rinsed with water followed by drying at 60 °C. We imaged the apatite formation via SEM. The mineral elements formed on the surface at day 7 were analyzed with EDS.

Adsorption and Release Assays. To absorb the growth factor rhBMP-2 on the surfaces of the composites membranes, four membranes were immersed in 5 mL of rhBMP-2 solutions (500 μg/mL) at room temperature for 4 h with gentle shaking. The membranes were then washed three times with phosphate-buffered saline (PBS; pH 7.4) and dried under a vacuum at room temperature for 48 h. The loading efficiency of rhBMP-2 into the membranes was evaluated by subtracting the amount of free rhBMP-2 from a control solution not exposed to the scaffold. The release experiment was conducted by incubating the scaffolds in 2 mL of PBS with 1% bovine serum albumin (BSA, Sigma) at 37 °C for up to 20 days at 50 rpm of agitation. The supernatant was collected periodically and replaced with fresh PBS. The rhBMP-2 in the samples was measured with an ELISA kit according to the manufacturer's protocol. Light absorbance was read with a plate reader at 450 nm.

Cell Proliferation. Cells were cultured in the α-MEM culture media supplemented with 10% fetal bovine serum (FBS), 1.0% penicillin (100 U/mL) and streptomycin sulfate (100 mg/mL) (GibcoBRL, Grand Island, NY). The cells were incubated at 37 °C in a humidified atmosphere of 5% CO_2 and 95% air. The growth medium was changed every 48 h. MSCs at passage 3 were detached by 0.25% trypsin, resuspended with fresh culture medium and used for the experiments described below.

One milliliter of the cell suspension at a cell density of 2×10^4 viable hMSCs was seeded into a 48-well plate (Costar3548, US) containing four different samples. The mixture was incubated at 37 °C in a humidified atmosphere of 5% CO_2 and 95% air. After 7 days, cells on the surfaces of the four samples were stained with 4′,6′-diamidino-2-phenylindole (DAPI, Biyuntian, Shanghai, China). The cells were observed using a fluorescence microscope (TE2000, Nikon, Japan).

The proliferation of hMSCs on the substrates was evaluated with a 3-(4,5-dimethylthiazol-2-yl)-2,5-diphenyltetrazolium bromide (MTT, Biyuntian, Shanghai, China) assay after 1, 3 and 7 days of culture.[36] Briefly, the substrates were placed into a 48-well plate and seeded with 1.0 mL of the cell suspension with cell density of 5×10^3 viable cells. We next added 100 μL of MTT. After the solution incubated at 37 °C, formazan formed and was dissolved in dimethyl sulfoxide (DMSO) for reading at 490 nm (Synergy HT, Biotek, USA). Controls included a medium-control well. This was used to correct the test absorbance values.[36] Five parallel experiments in each sample were conducted to statistically assess the cell proliferation.

Cell Attachment. The morphology of the adherent cells was evaluated after 3 and 24 h of culture by SEM. The membranes were gently removed from the culture and washed in PBS for 5 min to remove free cells and proteins. The cells were then fixed in 0.125% glutaraldehyde in distilled water. After the samples were incubated for 1 h at 4 °C, they were rinsed extensively with PBS and then dehydrated in increasing concentrations of ethanol (70, 90 and 100%) for 10 min each. After dehydration, the membranes were air-dried and characterized by SEM.

Cell morphology and alignment were studied by staining the filamentous actin of the cytoskeleton. After 24 h of incubation with the membranes, the cells on the surface of the membranes were rinsed three times with PBS and fixed with 4% paraformaldehyde for 20 min. The cells were permeabilized with 0.1% Triton X-100 in PBS for another 20 min. After washing thrice with PBS, the cells were incubated with fluorescein isothiocyanate−phalloidin (Sigma-Aldrich) for 1 h. After the cells were washed with PBS again, the cell nuclei were stained with DAPI. The cell morphology and alignment were visualized using confocal laser scanning microscopy (CLSM) (Nikon A1R, Nikon, Japan).

Cell Viability. Cell viability was evaluated using a live/dead assay kit (Abcam, Sigma-Aldrich) by following the manufacturer's instructions. Briefly, the cells and films were first washed twice with PBS and then incubated in the standard working solution at room temperature for 10 min. The samples were then washed again two times using PBS and observed under the confocal laser scanning microscopy (Nikon A1R, Nikon, Japan).

Osteogenic Differentiation of hMSCs. MSCs (3×10^4 cells/mL) were used to evaluate the effect of the membranes on the osteogenic differentiation. A 48-well plate without membranes was the blank control. After incubation in another 48-well plate with four substrates for 24 h, the culture medium in the above two sets of plates was changed to the osteogenic induction medium (OIM). The α-MEM was supplemented with 10% FBS, 0.1 μM dexamethasone (Sigma), 50 μM ascorbate acid (Sigma) and 10 mM β-glycerophosphate sodium (Sigma). These media were renewed every 2 days throughout the study period.

The ALP activity of the membranes was measured with and without BMP2. After 4, 7 and 14 days of osteogenic induction culture, the ALP activity was determined with a *p*-nitrophenyl phosphate (pNPP) (Sigma) assay. The total protein contents were measured with the bicinchoninic acid (BCA) method. The absorbance of the resulting *p*-nitrophenol was measured at 405 nm. The intracellular total protein content was measured with a MicroBCA protein assay kit. The ALP activity was normalized to the total protein content.

After 7 and 14 days of culture, the ALP was stained with a literature protocol.[37] In brief, the cells on the membranes were detached with 100 μL of a 0.25% trypsin solution and then transferred to another 48-well plate containing 1.0 mL of culture media to allow the cells to adhere. After 24 h, we stained with an ALP staining kit according to the manufacturer's instructions (Beyotime Biotech, Jiangsu, China). The cells were spread on the bottom of the well, rinsed twice with PBS, and then fixed using formalin for 30 s. After the cells were washed with distilled water twice, the cells were stained with a staining reagent for 60 min. Stained cells were photographed using a microscope (TE2000U, Nikon, Japan).

RESULTS AND DISCUSSION

Characterization of SBA15. Figure 1A shows a representative high resolution TEM image and BET analysis of SBA15 confirming an ordered array of silica structures with relatively uniform pore sizes (about 6 nm).

Typical small-angle X-ray diffraction (SAXRD) profiles of as-prepared SBA15 nanoparticles in the 2θ range from 0.5° to 6° are depicted in Figure 1B. Well-resolved peaks at 1.1° and weak peaks at 1.8° and 2.2° were attributed to (100), (110) and (200) Bragg diffractions and suggested a highly ordered hexagonal structure of SBA15.

We used nitrogen sorption analyses to measure the porosity of synthesized SBA15. The isotherms are type 4; they indicate steep, type H1 hysteresis at elevated pressures (see Figure 1C). This is normal for mesoporous materials with capillary condensation and evaporation as well as narrow size distributions. The surface area and pore volume of SBA15 are about 732 m^2/g and 1.2 cm^3/g, respectively.

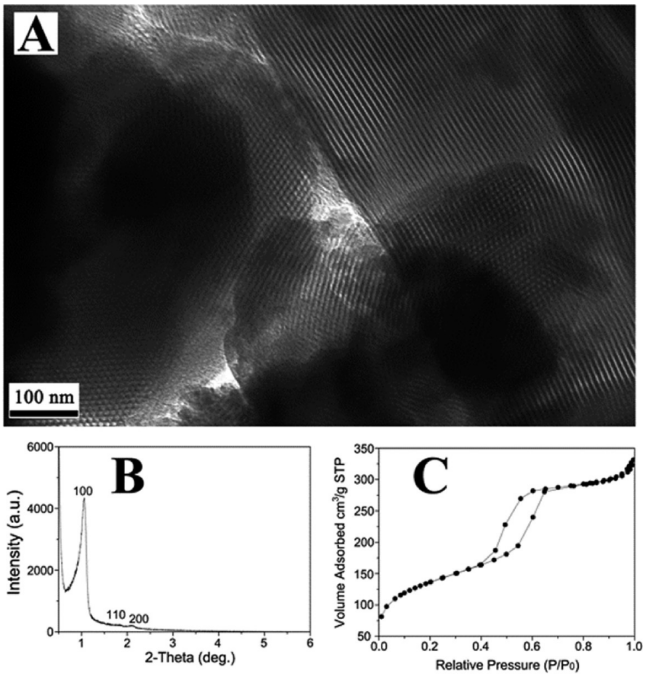

Figure 1. (A) TEM, (B) SAXRD and (C) BET analyses of SBA15.

Morphology of the Composite Membrane. SEM revealed the porous structures of the pure PLGA membrane and the PLGA−SBA15 composite membranes (Figure 2). In addition, BET analyses revealed that pure PLGA, PLGA-2.5% SBA, PLGA-5%SBA and PLGA-10%SBA porosities are 87.0%, 86.5%, 85.5% and 86.3%, respectively. As shown in Figure 2, the diameter of the nanofiber decreases as a function of percent SBA15. Also, Figure 2 confirms that the presence of SBA15 helps to form a net-like structure with even and irregularly distributed interconnected pores.

It is noteworthy that there are many beads on the pure PLGA membrane. Those beads are produced during the electrospinning of pure PLGA without SBA and are related to the polarity of polymer solution. When SBA15 was added, the polarity of the solution increased, leading to the decrease in the amount of beads.[38]

Energy Dispersive X-ray Spectrometry of Composite Membranes. Energy dispersive X-ray spectrometry (EDS) was used to determine the distribution of calcium and silicon on each membrane. Figure 3 indicates that the silicon was evenly distributed in each membrane. Indeed, SBA15 was also distributed evenly in the membrane, but silicon was significantly higher on the membrane with 10%SBA15 than that on other membranes, suggesting that excellent biomineralization may be induced on the membrane with 10% SBA15.

Absorption and Sustained Release of rhBMP-2. The amount of BMP-2 absorbed on the membrane was measured using ELISA. Figure 4A indicates that the amount of BMP-2 loaded on the membrane of pure PLGA, PLGA-2.5%SBA15, PLGA-5%SBA15 or PLGA-10%SBA15 was 17.04 ± 1.36 μg/mg, 18.23 ± 2.44 μg/mg, 19.45 ± 2.4 μg/mg and 21.53 ± 1.3 μg/mg. All quantitative data were analyzed by Origin 8.0 (OriginLab Corporation). Statistical comparisons were carried out using analysis of variance (ANOVA). The statistical significance was considered greater than 95% confidence level ($p < 0.05$). The amount of BMP-2 loaded in the other groups (PLGA-2.5%SBA15, PLGA-5%SBA15 or PLGA-10%SBA15)

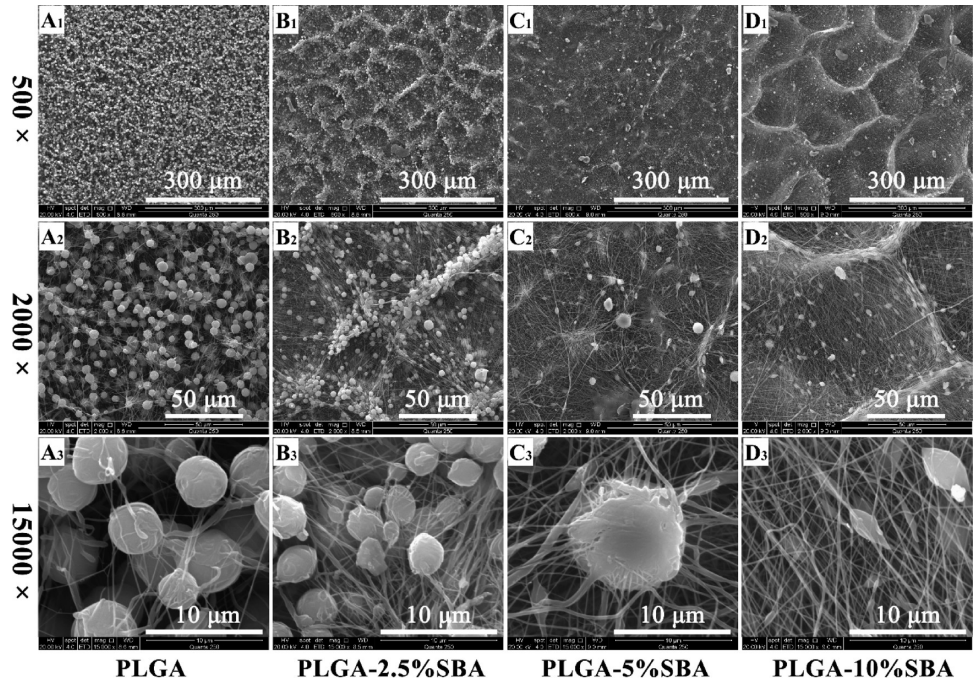

Figure 2. SEM images of pure PLGA membrane and PLGA−SBA15 composite membranes: (A_1−A_3) pure PLGA without SBA15; (B_1−B_3) PLGA-2.5%SBA15; (C_1−C_3) PLGA-5%SBA15; (D_1−D_3) PLGA-10%SBA15.

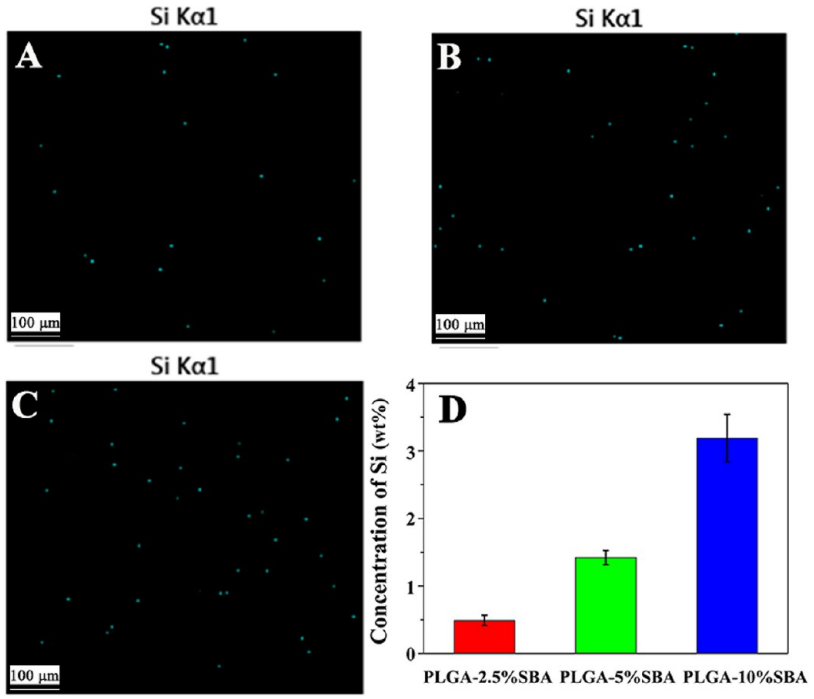

Figure 3. EDS mapping of the silicon in the PLGA−SBA15 composite membranes: (A) PLGA-2.5%SBA15; (B) PLGA-5%SBA15; (C) PLGA-10% SBA15 and (D) silicon distribution.

was significantly higher than that on the pure PLGA membrane. Also, the amount of BMP-2 on PLGA-10%SBA15 membrane was the highest indicating that SBA15 enhances the absorption of BMP-2 onto the membranes.

The release rates of BMP-2 from the three PLGA−SBA15 composite membranes were slower than that from the pure PLGA membrane. The slowest rate was from the PLGA-10% SBA15 membrane, suggesting that the presence of SBA15 optimizes BMP-2 release. Although the presence of SBA15 did not significantly affect the release kinetics of BMP-2, it did prolong the local retention of the growth factor. This is because mesoporous silica materials have many pores and channels which are beneficial for delivering and release of biologically active ingredients.[39] Furthermore, SBA-15 has advantages as carriers to provide a sustained and localized release of therapeutically relevant factors.[40] Figure 4 suggests that the incorporation of rhBMP-2 into the SBA-15 nanoparticles may reduce its initial burst release and prolong residence time in the

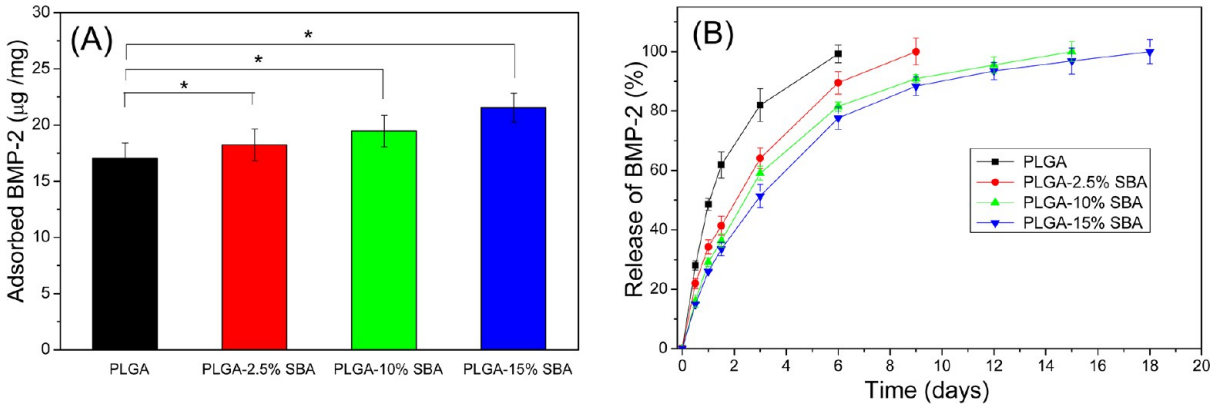

Figure 4. (A) rhBMP-2 adsorption on the pure PLGA membranes and the PLGA−SBA15 composite membranes. The amount of rhBMP-2 adsorbed on the membranes with different contents of SBA15 after 4 h of incubation with rhBMP-2 solutions ($p < 0.05$); (B) release of rhBMP-2 from the pure PLGA and PLGA−SBA15 membranes showing the released amount of rhBMP-2 adsorbed on the membranes with various amounts of SBA15 after 20 days of incubation in PBS ($p < 0.05$).

body and thereby overcome the inherent problem associated with traditional scaffold materials.

Cell Proliferation. The cell densities counted via DAPI staining (Figure 5) on the PLGA-2.5%SBA15 (B), PLGA-5%

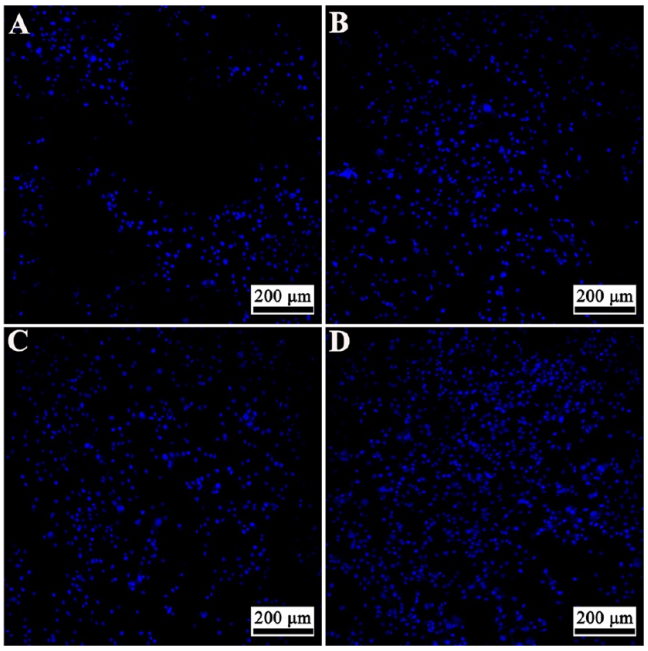

Figure 5. CLSM images of hMSCs cultured on the PLGA and PLGA−SBA15 composite membranes after 7 days: (A) pure PLGA; (B) PLGA-2.5%SBA15; (C) PLGA-5%SBA15; (D) PLGA-10%SBA15 membranes.

SBA15 (C) and PLGA-10%SBA15 (D) membranes were all higher than that on the pure PLGA membrane (A). In addition, the cell density on the PLGA-10%SBA15 membrane was very high, indicating that the presence of SBA15 facilitated the proliferation of hMSCs.

The cell proliferation was also examined using the MTT assay (Figure 6). After 1 and 3 days of culture, the amount of cells on the membranes showed no significant differences. After 7 days of culture, the amount of cells on the PLGA-10%SBA15 membrane was higher than that on the pure PLGA membrane,

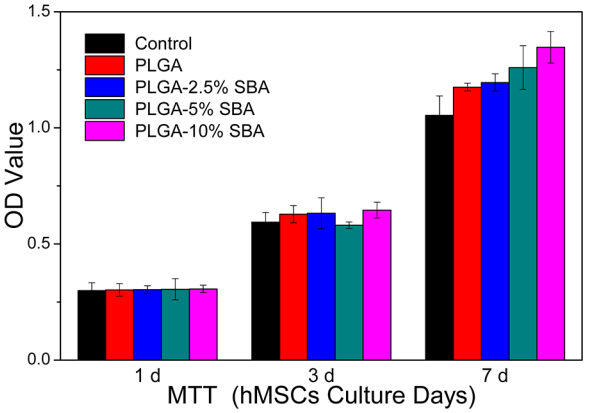

Figure 6. Proliferation of hMSCs on the PLGA−SBA15 membranes after 1, 3 and 7 days of culture.

suggesting that the presence of SBA15 can promote the proliferation of hMSCs.

In Figure 5, we see that the amount of cells in pure PLGA is less than that for the other groups. However, there are no significant differences between the groups (Figure 6), i.e., the cell viability and the cell proliferation results are consistent.

Cell Attachment. The hMSC morphology and spreading to the PLGA−SBA15 nanofibrous membranes at different time intervals (3 and 24 h) were viewed by SEM (Figure 7). The cells on the pure PLGA membrane did not spread after 3 h. In contrast, the cells on the membranes with SBA15 had a more elongated morphology. After 24 h of culture, more extensive spreading and flattening of hMSCs were observed on the PLGA−SBA15 membrane versus the pure PLGA membrane. Also, the PLGA-10%SBA15 membrane showed the best attachment and spreading of hMSCs.

Figure 8 shows that the cells spread on the pure PLGA. The PLGA−SBA15 composite membranes had an irregular polygonal shape, suggesting that the cells spread well on the membranes. The amount of cells as well as actin filaments on the PLGA-10%SBA15 membrane was higher than those on the pure PLGA membrane, indicating excellent cell adhesion to PLGA-10%SBA15 membrane. Overall, the presence of SBA15 improved the adsorption of cells on the membrane and facilitated the attachment and spread of cells on the membranes.

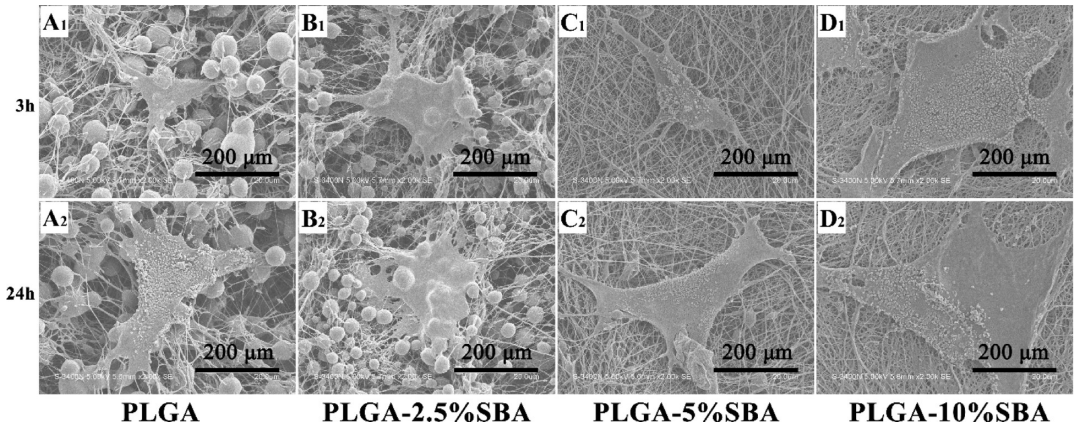

Figure 7. SEM images of the attachment of hMSCs to the membranes showing the cell attachment and spreading after 3 and 24 h: (A_1–A_2) pure PLGA; (B_1–B_2) PLGA-2.5%SBA15; (C_1–C_2) PLGA-5%SBA15; (D_1–D_2) PLGA-10%SBA15.

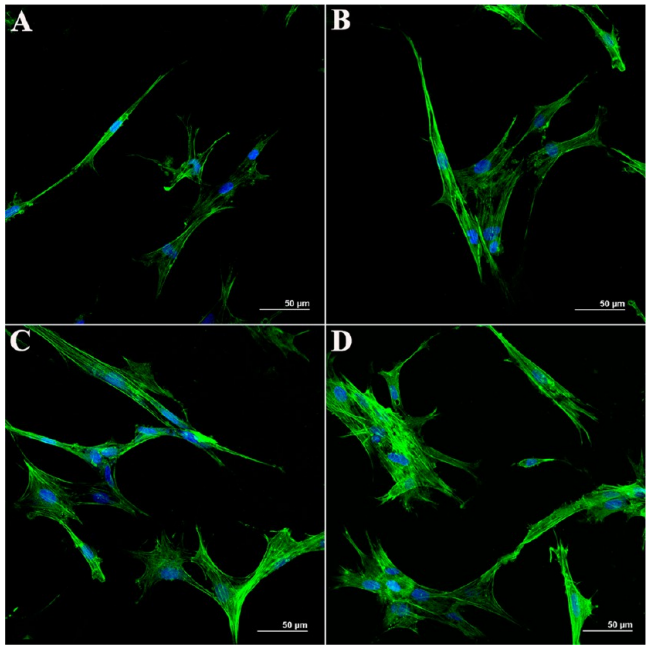

Figure 8. Cellular morphology and alignment of the hMSCs on different membranes: (A) pure PLGA; (B) PLGA-2.5%SBA15; (C) PLGA-5%SBA15; (D) PLGA-10%SBA15. Cellular actin filaments stained with fluorescein isothiocyanate–phalloidin (green) and nuclei counterstained with 4′,6′-diamidino-2-phenylindole (blue).

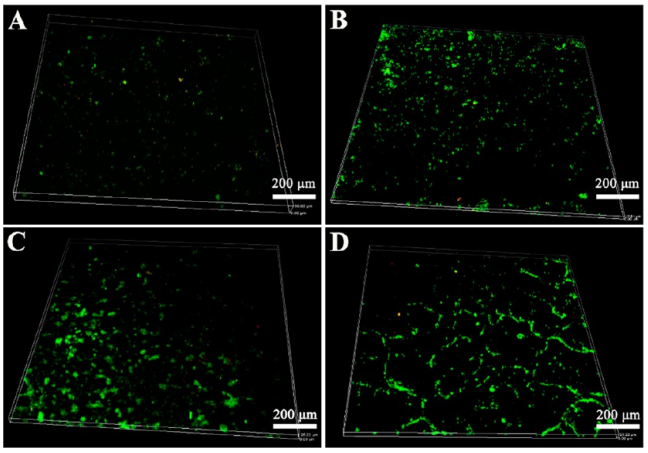

Figure 9. Viability of hMSCs on the PLGA–SBA15 membranes. The CLSM images show cell viability after incubation on the membranes for 7 days. (A) Pure PLGA; (B) PLGA-2.5%SBA15; (C) PLGA-5% SBA15; (D) PLGA-10%SBA15. Live cells are green; dead cells are red.

Cell Viability. The CLSM images in Figure 9A shows good cell viability on the pure PLGA membrane. The addition of SBA15 can further improve the cell viability (Figure 9B–D). More cell survival occurs on membranes with SBA15 versus pure PLGA. Cells on the PLGA-10%SBA15 membrane showed the best viability and maintained a fibroblast-like morphology during culture. These data suggest that the PLGA–SBA15 membranes were not cytotoxic.

Differentiation of hMSCs. We measured ALP levels in hMSCs stimulated by osteogenic medium and unstimulated cells.

Figure 10A presents the ALP levels in the absence of rhBMP-2. The ALP staining intensity on the PLGA-10%SBA15 membrane was significantly increased on day 14 versus days 4 and 7. Because the ALP activity was measured as a marker of differentiation of hMSCs and also of osteoblastic phenotype expression, the above results indicate that PLGA–SBA15 membranes can facilitate the differentiation of hMSCs into osteoblasts.

The ALP activities on the membranes in the presence of rhBMP-2 are shown in Figure 10B. There was no significant difference in the ALP staining between the membranes on day 4 after culture. However, there was a significant increase in the ALP staining intensity on the PLGA-10%SBA15 membrane with rhBMP-2 versus the blank control as well as the pure PLGA membrane on days 7 and 14. This confirms that SBA15 optimizes the sustained release of BMP-2.

The ALP staining results after 7 and 14 days of cell culture are shown in Figure 11. The faint positive staining of ALP was observed on each membrane on day 7, and the intensity of the ALP staining on each membrane was enhanced significantly on day 14. It is noteworthy that the ALP staining intensity on the PLGA-10%SBA15 membrane was higher than that on the pure PLGA membrane. This suggests that SBA15 can improve the differentiation of hMSCs into osteoblasts.

An excellent membrane for bone tissue engineering should possess a structure similar to the extracellular matrix in bone. Studies have demonstrated that well-interconnected microporous structures and appropriate pore sizes are very important to interaction between the cells. They can facilitate the proliferation as well as the attachment of the cells.[41,42] These

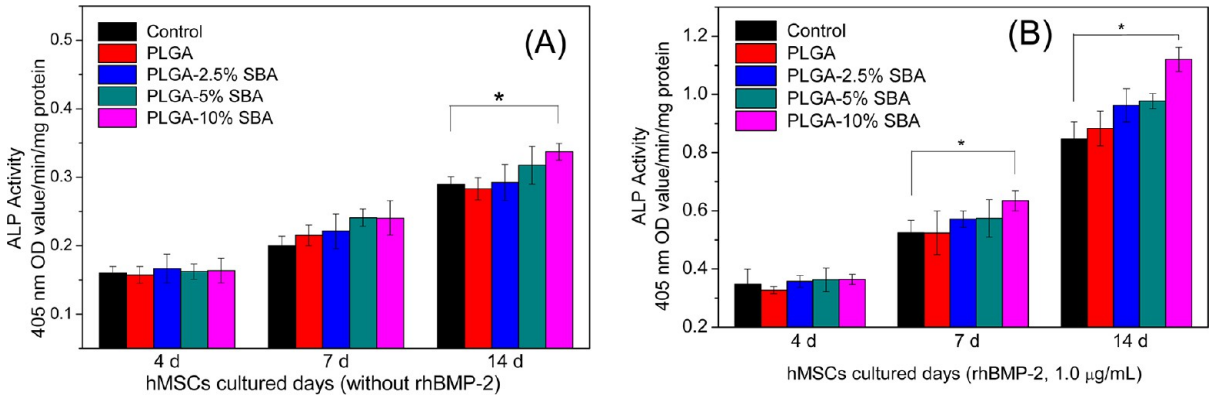

Figure 10. (A) ALP activity in the absence of rhBMP-2: comparison of the alkaline phosphatase activity of hMSCs from day 1 to day 14 in culture. Here, an asterisk indicates significant differences from that of PLGA-10% SBA group ($p < 0.05$). (B) ALP activity assay in the presence of rhBMP-2: comparison of the alkaline phosphatase activity of hMSCs from day 1 to day 14 in culture. Here, an asterisk indicates significant differences from that of untreated cells ($p < 0.05$).

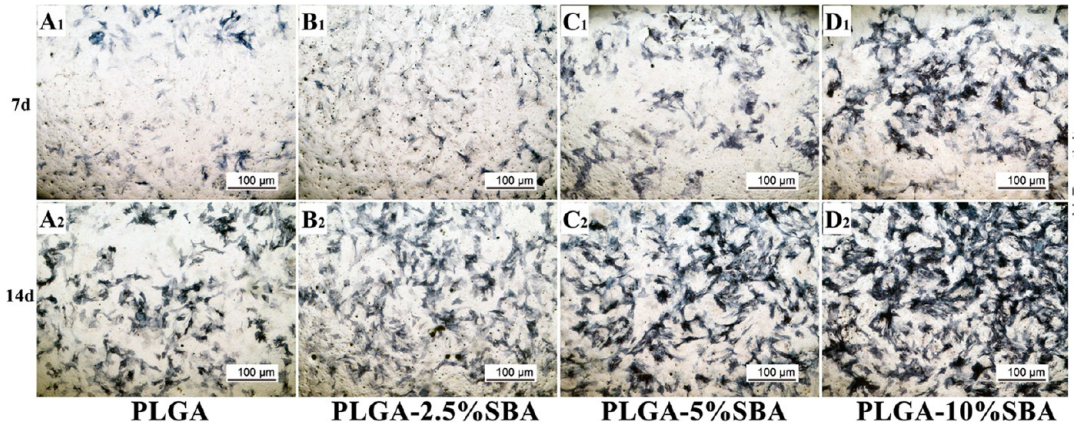

Figure 11. ALP staining of hMSCs after 7 and 14 days of culture with the osteogenic induction medium in the presence of rhBMP-2: (A_1–A_2) PLGA; (B_1–B_2) PLGA-2.5%SBA15; (C_1–C_2) PLGA-5%SBA15; (D_1–D_2) PLGA-10%SBA15.

factors play a direct role in the transportation of oxygen and nutrients needed by cells.[43] In our study, the membranes possessed an interconnected microporous structure. These features can facilitate the transportation of nutrients to cells.

The analysis of the BMP adhesion to the membrane and the release from the membranes showed that the PLGA–SBA15 membranes can absorb more proteins and prolong the release of the proteins versus the pure PLGA membrane. This might be due to the larger surface area formed by SBA15 on the surface of the PLGA–SBA15 membranes. Furthermore, the sustained release of rhBMP-2 will improve bone healing.[44]

The analysis of cell proliferation, attachment, and viability showed that SBA15 is nontoxic and promotes cell proliferation and attachment. The PLGA–SBA15 composite membranes have excellent biocompatibility. The enhanced proliferation of MSCs on the PLGA–SBA15 composite membrane may be related to the direct contact of the seeded cells with the SBA15 particles on the scaffold surface. This might provide better cell adhesion sites that promote cell spreading and proliferation.

The ALP study indicated that the PLGA–SBA15 membrane is better for osteogenic differentiation than the pure PLGA membrane and has excellent bioactivity in vivo. This is probably because SBA15 contains silicon and silicon dioxide that are osteoinductive and a catalyst for bone formation.[45]

CONCLUSIONS

In conclusion, we have successfully prepared PLGA–SBA15 composite membranes with different silica contents by electrospinning. The TEM, BET and SAXRD studies confirmed that SBA15 has a mesoporous structure and a large surface area. The EDS results revealed that the SBA15 was distributed evenly in the PLGA–SBA15 composite membranes. SEM confirmed the well-interconnected pore structure of the PLGA–SBA15 composite membranes that can facilitate cell growth and spreading. The presence of SBA15 can enhance the rhBMP-2 adhesion to the membrane and optimizes the sustained release of rhBMP-2 from the membrane. The cells seeded on the PLGA–SBA15 composite membrane had excellent proliferation and attachment suggesting that the membrane has excellent biocompatibility. Moreover, this composite membrane can improve the ALP activity in hMSCs. Furthermore, the composite membrane with absorbed rhBMP-2 can induce excellent ectopic bone formation with excellent bioactivity. Overall, the PLGA–SBA15 composite membranes prepared by electrospinning are a promising material for bone repair.

AUTHOR INFORMATION

Corresponding Authors

*S. Xu. E-mail: shuogui126@126.com.

*J. Du. E-mail: jzdu@tongji.edu.cn. Tel: +86-21-6958-0239. Fax: +86-21-6958-4723.

Author Contributions

[§]These authors contributed equally to the paper.

Notes

The authors declare no competing financial interest.

■ ACKNOWLEDGMENTS

J.D. is supported by National Natural Science Foundation of China (21174107 and 21374080), Eastern Scholar Professorship (P2009011) and Shanghai 1000 Plan (SH01068).

■ REFERENCES

(1) Wang, H. N.; Li, Y. B.; Zuo, Y.; Li, J. H.; Ma, S. S.; Cheng, L. Biocompatibility and Osteogenesis of Biomimetic Nano-Hydroxyapatite/Polyamide Composite Scaffolds for Bone Tissue Engineering. *Biomaterials* **2007**, *28*, 3338−3348.

(2) Hollister, S. J. Porous Scaffold Design for Tissue Engineering. *Nat. Mater.* **2005**, *4*, 518−524.

(3) Vats, A.; Tolley, N. S.; Polak, J. M.; Gough, J. E. Scaffolds and Biomaterials for Tissue Engineering: A Review of Clinical Applications. *Clin. Otolaryngol.* **2003**, *28*, 165−172.

(4) Nitya, G.; Nair, G. T.; Mony, U.; Chennazhi, K. P.; Nair, S. V. In Vitro Evaluation of Electrospun PCL/Nanoclay Composite Scaffold for Bone Tissue Engineering. *J. Mater. Sci.: Mater. Med.* **2012**, *23*, 1749−1761.

(5) Jose, M. V.; Thomas, V.; Johnson, K. T.; Dean, D. R.; Nyalro, E. Aligned PLGA/HA Nanofibrous Nanocomposite Scaffolds for Bone Tissue Engineering. *Acta Biomater.* **2009**, *5*, 305−315.

(6) Karp, J. M.; Shoichet, M. S.; Davies, J. E. Bone Formation on Two-Dimensional (DL-Lactide-co-Glycolide) (PLGA) Films and Three-Dimensional PLGA Tissue Engineering Scaffolds in vitro. *J. Biomed. Mater. Res., Part A* **2003**, *64A*, 388−396.

(7) Anderson, J. M.; Shive, M. S. Biodegradation and Biocompatibility of PLA and PLGA Microspheres. *Adv. Drug Delivery Rev.* **1997**, *28*, 5−24.

(8) Ngiam, M.; Liao, S. S.; Patil, A. J.; Cheng, Z. Y.; Chan, C. K.; Ramakrishna, S. The Fabrication of Nano-Hydroxyapatite on PLGA and PLGA/Collagen Nanofibrous Composite Scaffolds and Their Effects in Osteoblastic Behavior for Bone Tissue Engineering. *Bone* **2009**, *45*, 4−16.

(9) Tao, C.; Huang, J.; Lu, Y.; Zou, H.; He, X.; Chen, Y.; Zhong, Y. Development and Characterization of GRGDSPC-Modified Poly-(Lactide-co-Glycolide Acid) Porous Microspheres Incorporated with Protein-Loaded Chitosan Microspheres for Bone Tissue Engineering. *Colloids Surf., B* **2014**, *122*, 439−446.

(10) Kempen, D. H. R.; Lu, L. C.; Heijink, A.; Hefferan, T. E.; Creemers, L. B.; Maran, A.; Yaszemski, M. J.; Dhert, W. J. A. Effect of Local Sequential VEGF and BMP-2 Delivery on Ectopic and Orthotopic Bone Regeneration. *Biomaterials* **2009**, *30*, 2816−2825.

(11) Lee, J. W.; Kang, K. S.; Lee, S. H.; Kim, J. Y.; Lee, B. K.; Cho, D. W. Bone Regeneration Using a Microstereolithography-Produced Customized Poly(Propylene Fumarate)/Diethyl Fumarate Photopolymer 3D Scaffold Incorporating BMP-2 Loaded PLGA Microspheres. *Biomaterials* **2011**, *32*, 744−752.

(12) Betz, O. B.; Betz, V. M.; Abdulazim, A.; Penzkofer, R.; Schmitt, B.; Schroder, C.; Mayer-Wagner, S.; Augat, P.; Jansson, V.; Muller, P. E. The Repair of Critical-Sized Bone Defects Using Expedited, Autologous BMP-2 Gene-Activated Fat Implants. *Tissue Eng., Part A* **2010**, *16*, 1093−1101.

(13) Kong, S. W.; Kim, J. S.; Park, K. S.; Cha, B. H.; Shim, J. H.; Kim, J. Y.; Cho, D. W.; Rhie, J. W.; Lee, S. H. Surface Modification with Fibrin/Hyaluronic Acid Hydrogel on Solid-Free Form-Based Scaffolds Followed by BMP-2 Loading to Enhance Bone Regeneration. *Bone* **2011**, *48*, 298−306.

(14) Liu, W. C.; Robu, I. S.; Patel, R.; Leu, M. C.; Velez, M.; Gabriel Chu, T. M. The Effects of 3D Bioactive Glass Scaffolds and BMP-2 on Bone Formation in Rat Femoral Critical Size Fefects and Adjacent Bones. *Biomed. Mater.* **2014**, *9*, 045013.

(15) Kong, X.; Wang, J.; Cao, L.; Yu, Y.; Liu, C. Enhanced Osteogenesis of Bone Morphology Protein-2 in 2-N,6-O-Sulfated Chitosan Immobilized PLGA Scaffolds. *Colloids Surf., B* **2014**, *122*, 359−367.

(16) Izquierdo-Barba, I.; Ruiz-Gonzalez, L.; Doadrio, J. C.; Gonzalez-Calbet, J. M.; Vallet-Regi, M. Tissue Regeneration: A New Property of Mesoporous Materials. *Solid State Sci.* **2005**, *7*, 983−989.

(17) Vallet-Regi, M.; Colilla, M.; Gonzalez, B. Medical Applications of Organic-Inorganic Hybrid Materials Within the Field of Silica-Based Bioceramics. *Chem. Soc. Rev.* **2011**, *40*, 596−607.

(18) Jones, J. R. Review of Bioactive Glass: from Hench to Hybrids. *Acta Biomater.* **2013**, *9*, 4457−4486.

(19) Madhugiri, S.; Dalton, A.; Gutierrez, J.; Ferraris, J. P.; Balkus, K. J. Electrospun MEH-PPV/SBA-15 Composite Nanofibers Using a Dual Syringe Method. *J. Am. Chem. Soc.* **2003**, *125*, 14531−14538.

(20) Li, X.; Wang, X.; Zhang, L.; Chen, H.; Shi, J. MBG/PLGA Composite Microspheres with Prolonged Drug Release. *J. Biomed. Mater. Res., Part B* **2009**, *89*, 148−154.

(21) Wu, C. T.; Zhou, Y. H.; Xu, M. C.; Han, P. P.; Chen, L.; Chang, J.; Xiao, Y. Copper-Containing Mesoporous Bioactive Glass Scaffolds with Multifunctional Properties of Angiogenesis Capacity, Osteostimulation and Antibacterial Activity. *Biomaterials* **2013**, *34*, 422−433.

(22) Scarber, R. E.; Salaam, A. D.; Thomas, V.; Janowski, G. M.; Dean, D. Direct Sol-Gel Electrospinning of Fibrous Bioglass Scaffolds for Bone Tissue Engineering. *J. Biomater. Tissue Eng.* **2013**, *3*, 440−447.

(23) Tong, H. W.; Wang, M. Negative Voltage Electrospinning of Fibrous Nanocomposite Scaffolds for Bone Tissue Engineering. *J. Aust. Ceram. Soc.* **2012**, *48*, 38−43.

(24) Yoshimoto, H.; Shin, Y. M.; Terai, H.; Vacanti, J. P. A Biodegradable Nanofiber Scaffold by Electrospinning and its Potential for Bone Tissue Engineering. *Biomaterials* **2003**, *24*, 2077−2082.

(25) Liao, S.; Li, B. J.; Ma, Z. W.; Wei, H.; Chan, C.; Ramakrishna, S. Biomimetic Electrospun Nanofibers for Tissue Regeneration. *Biomed. Mater.* **2006**, *1*, R45−R53.

(26) Shin, M.; Yoshimoto, H.; Vacanti, J. P. In vivo Bone Tissue Engineering Using Mesenchymal Stem Cells on a Novel Electrospun Nanofibrous Scaffold. *Tissue Eng.* **2004**, *10*, 33−41.

(27) Min, B. M.; Lee, G.; Kim, S. H.; Nam, Y. S.; Lee, T. S.; Park, W. H. Electrospinning of Silk Fibroin Nanofibers and its Effect on the Adhesion and Spreading of Normal Human Keratinocytes and Fibroblasts in vitro. *Biomaterials* **2004**, *25*, 1289−1297.

(28) Zhao, D. Y.; Huo, Q. S.; Feng, J. L.; Chmelka, B. F.; Stucky, G. D. Nonionic Triblock and Star Diblock Copolymer and Oligomeric Surfactant Syntheses of Highly Ordered, Hydrothermally Stable, Mesoporous Silica Structures. *J. Am. Chem. Soc.* **1998**, *120*, 6024−6036.

(29) Zhu, Y. Q.; Wang, F. Y. K.; Zhang, C.; Du, J. Z. Preparation and Mechanism Insight of Nuclear Envelope-like Polymer Vesicles for Facile Loading of Biomacromolecules and Enhanced Biocatalytic Activity. *ACS Nano* **2014**, *8*, 6644−6654.

(30) Zhu, Y. Q.; Fan, L.; Yang, B.; Du, J. Z. Multifunctional Homopolymer Vesicles for Facile Immobilization of Gold Nanoparticles and Effective Water Remediation. *ACS Nano* **2014**, *8*, 5022−5031.

(31) Liu, Q. M.; Chen, J.; Du, J. Z. Asymmetrical Polymer Vesicles with a "Stealthy" Outer Corona and an Endosomal-Escape-Accelerating Inner Corona for Efficient Intracellular Anticancer Drug Delivery. *Biomacromolecules* **2014**, *15*, 3072−3082.

(32) Xiao, J.; Chen, W. Q.; Wang, F. Y. K.; Du, J. Z. Polymer/TiO_2 Hybrid Nanoparticles with Highly Effective UV-Screening but Eliminated Photocatalytic Activity. *Macromolecules* **2013**, *46*, 375−383.

(33) Du, J. Z.; Sun, H. Polymer/TiO_2 Hybrid Vesicles for Excellent UV Screening and Effective Encapsulation of Antioxidant Agents. *ACS Appl. Mater. Interfaces* **2014**, *6*, 13535−13541.

(34) Yang, F.; Both, S. K.; Yang, X. C.; Walboomers, X. F.; Jansen, J. A. Development of an Electrospun Nano-apatite/PCL Composite

Membrane for GTR/GBR Application. *Acta Biomater.* **2009**, *5*, 3295−3304.
(35) Kokubo, T.; Kushitani, H.; Sakka, S.; Kitsugi, T.; Yamamuro, T. Solutions Able to Reproduce in vivo Surface-Structure Changes in Bioactive Glass-Ceramic A-W. *J. Biomed. Mater. Res.* **1990**, *24*, 721−734.
(36) Tan, H. L.; Guo, S. R.; Yang, S. B.; Xu, X. F.; Tang, T. T. Physical Characterization and Osteogenic Activity of the Quaternized Chitosan-Loaded PMMA Bone Cement. *Acta Biomater.* **2012**, *8*, 2166−2174.
(37) Sugiyama, O.; Orimo, H.; Suzuki, S.; Yamashita, K.; Ito, H.; Shimada, T. Bone Formation Following Transplantation of Genetically Modified Primary Bone Marrow Stromal Cells. *J. Orthop. Res.* **2003**, *21*, 630−637.
(38) Wang, S. G.; Li, Y. X.; Wang, Y. Z.; Yang, Q. B.; Wei, Y. Introducing CTAB into CdTe/PVP Nanofibers Enhances the Photoluminescence Intensity of CdTe Nanoparticles. *Mater. Lett.* **2007**, *61*, 4674−4678.
(39) Liu, X. Y.; Zhu, L.; Zhao, T.; Lan, J. F.; Yan, W. F.; Zhang, H. X. Synthesis and Characterization of Sulfonic Acid-Functionalized SBA-15 for Adsorption of Biomolecules. *Microporous Mesoporous Mater.* **2011**, *142*, 614−620.
(40) Zhou, P.; Xia, Y.; Cheng, X.; Wang, P.; Xie, Y.; Xu, S. Enhanced Bone Tissue Regeneration by Antibacterial and Osteoinductive Silica-HACC-Zein Composite Scaffolds Loaded with rhBMP-2. *Biomaterials* **2014**, *35*, 10033−10045.
(41) Hutmacher, D. W. Scaffolds in Tissue Engineering Bone and Cartilage. *Biomaterials* **2000**, *21*, 2529−2543.
(42) Zhang, R. Y.; Ma, P. X. Poly(alpha-Hydroxyl Acids) Hydroxyapatite Porous Composites for Bone-Tissue Engineering. I. Preparation and Morphology. *J. Biomed. Mater. Res.* **1999**, *44*, 446−455.
(43) Zhao, J.; Lu, X.; Weng, J. Macroporous Ti-Based Composite Scaffold Prepared by Polymer Impregnating Method with Calcium Phosphate Coatings. *Mater. Lett.* **2008**, *62*, 2921−2924.
(44) Fu, Y. C.; Nie, H.; Ho, M. L.; Wang, C. K.; Wang, C. H. Optimized Bone Regeneration Based on Sustained Release from Three-Dimensional Fibrous PLGA/HAp Composite Scaffolds Loaded with BMP-2. *Biotechnol. Bioeng.* **2008**, *99*, 996−1006.
(45) Vallet-Regi, M.; Balas, F.; Colilla, M.; Manzano, M. Bone-Regenerative Bioceramic Implants with Drug and Protein Controlled Delivery Capability. *Prog. Solid State Chem.* **2008**, *36*, 163−191.